



## BETHE-BLOCH ENERGY LOSS

Fluorescence-based detectors are being used in many places and the design of this system is based on several others [8,9,10]. Residual or injected gas is excited by the beam, and subsequent de-excitation produces light that can be imaged with sufficient resolution and small enough error to measure the beam width without fully stopping or intercepting the beam. A small gas bottle with an actuatable low pressure Festo valve for can be used for local gas puffing. Nitrogen gas is often used and emits well in the 390-470 nm range at pressures of  $\sim 10^{-6}$  Torr. The residual pressure of target gas has been estimated to be on this order, which has led to the additional baseline consideration of deuterium or helium gas. The space charge motion of ionized gas prior to re-emission of the photons can lead to blurring, but with the relaxation time for emission on order of 100 ns there is little time for movement, and the broadening due to drift is estimated at  $<30$  microns following [10] and should not dominate the mm scale measurement.

The cross-section for electromagnetic interaction of the beam is small at several MeV, or equivalently the stopping power of low pressure gas on an MeV scale deuteron beam is small. The beam energy loss is estimated using SRIM [11] calculations based on the Bethe-Bloch formula, and is shown in Fig. 3. The differential energy loss and stopping range is plotted as a function of energy at a pressure of 1 atmosphere of helium. This result shows the long stopping distance at even high pressure for energetic deuterons. Scaling this result to  $10^{-6}$  Torr requires simply multiplying by the different number density for the lower pressure. The average beam current of 300 micro Amps and  $dE/dx$  at 7 MeV allows a total energy loss into a 100 micron slice to be calculated at  $1.47 \times 10^{-11}$  W.

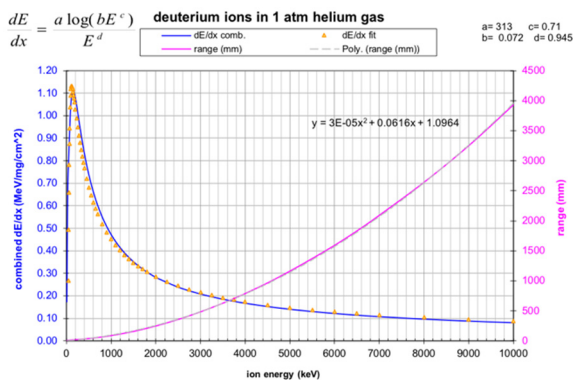


Figure 3: SRIM [11] output for energy loss in deuterium gas. Energy loss is scaled to the amount of gas seen by the beam and imageable by the diagnostic design.

## BEAMLINE LAYOUT

The fluorescence diagnostic chamber, or “Beam Imaging Diagnostic” (BID) is shown in Fig. 4. The BID is a spherical octagon attached to a 6-way vacuum cross that houses the insertable full power beam dump, described in [6]. The ports on the octagon opposite optical windows are terminated by standard length nipples and blanks that have

been blackened using an oxide coating to reduce the surface reflection from  $>60\%$  to  $<10\%$ . Further blackening has been investigated, if wall reflections continue to be a concern, such as in [10]. Carbon nanotube-based coatings or simple acetylene flame carbon coatings have been measured and show reflections below 1-2%.



Figure 4: Assembled BID chamber. Visible from left to right: in-flange ACCT, bellows with X-Y steerer, 4-way X-Y BPM, blackened through ports on imaging octagon, 6-way cross housing full power beam dump and turbomolecular pumping, temporary beam dump with ceramic stand-offs for Faraday cup measurement of current including a cooling fan.

The reflectivity was measured by spectrophotometer as a function of wavelength for 4 differently treated samples: standard stainless steel, black oxide coated, a flatter black oxide treatment obtained by bead-blasting the sample prior to coating, and a “superblack” coating that used an acetylene flame for carbon deposition. Results are shown in Fig. 5. The robustness of these coatings in the environment of differential pumping, and gas flows is of equal concern, and more aggressive blackening will only be used if it is measured to be necessary for more accurate measurements. Vertical and horizontal planes will be imaged separately, as well as a view at 45 degrees for confirmation of beam rotation at focus or asymmetry. The final focus tune has very nearly equal  $\beta_x$  and  $\beta_y$ , as seen in Fig. 1, but it is quite possible given the dipole bend in the horizontal plane that there will be different emittance growth or cross-coupling between the two directions. The 45 degree view will provide the ability to decouple the two dimensions, or tune them separately if necessary.

Content from this work may be used under the terms of the CC BY 3.0 licence (© 2019). Any distribution of this work must maintain attribution to the author(s), title of the work, publisher, and DOI

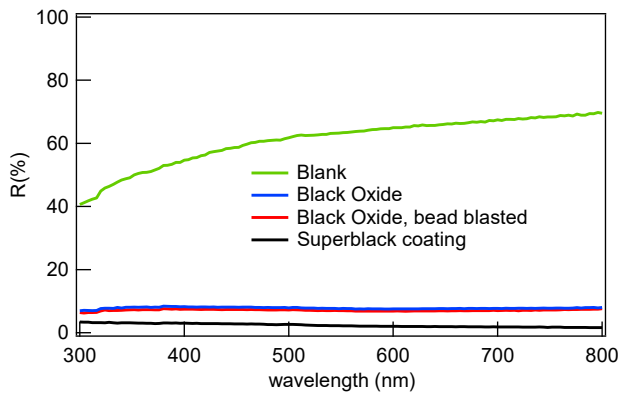


Figure 5: Reflection measurement for stainless steel vacuum blank, black oxide coatings, and superblack coating as a function of wavelength.

Other beamline diagnostics will complement the beam imaging and allow for fluorescence scaling. The beam current will be measured using alternating-current current transformers, and beam position will be measured using button-based 4-way beam position monitors. Pressure will be measured using a variety of sensors across a very large span of scales:  $10^3$  Torr to  $10^{-9}$  Torr. This range encompasses the high-pressure gas targets at above atmospheric pressure to the ultra-high vacuum possible in the accelerating structures.

## OPTICAL DESIGN

Only some of the energy lost by the deuteron beam is eventually converted into fluorescent light ( $\sim 1\%$ ). Uniform emission and optical layout geometry means small ( $10^{-4}$ ) solid angle collection of emitted light. These factors combine with the  $1.47 \times 10^{-11}$  W energy loss from the beam to yield  $\sim 30$  photons per 100 micron beam slice in the beam direction. This small number of photons per slice will yield acceptable statistics for slice width measurements, but will require single photon detection methods.

For beam profile measurements, the depth of field must subtend the beam diameter in order to minimize broadening. A resolution of 0.1 mm is deemed acceptable for imaging the beam diameter of 1-2 mm with sufficient data for profile fitting and width estimation. A two-stage multi-channel plate will be required in order to provide sufficient gain ( $10^6$ ) to image the single photon level signals expected from fluorescence. An integrated camera is preferred in order to minimize the operational impact from neutron-damaged electronics and maximize commercial support for component replacement in the future. Camera specification, vendor selection, and procurement is underway.

## CONCLUSION

First deuteron beam will be generated in 2019, and imaging with the fluorescence diagnostic will confirm initial and transported beam quality. Quadrupole magnet controls, Gauss probe calibrations and stability will be confirmed using beam-based measurements. The final focus will be adjusted and performance expectations will be established using this data as input into both beam dynamics modeling

and other machine constraints such as beam apertures and target design. Cross-calibration between upstream and downstream diagnostics will be used to characterize the beam at final focus so that the upstream settings can be confirmed in the future when the final neutron production target replaces the diagnostic.

## REFERENCES

- [1] J. Hall, F. Dietrich, C. Logan, and G. Schmid, "Development of high-energy neutron imaging for use in NDE applications", UCRL-JC-134562, SPIE 3769, 31 (1999).
- [2] M. S. Johnson *et al.*, "Development of a high-brightness, quasi-monoenergetic neutron source for neutron imaging", in *Proc. 2016 Conference on the Application of Accelerators in Research and Industry*, Ft. Worth, TX, USA.
- [3] B. Rusnak *et al.*, "Development of a high brightness source for fast neutron imaging", in *Proc. North American Particle Accelerator Conf. (NAPAC'16)*, Chicago, IL, USA, Oct. 2016, pp. 1260-1264. doi:10.18429/JACoW-NA-PAC2016-THB3I001
- [4] B. Rusnak *et al.*, "Advancement of an accelerator-driven high-brightness source for fast neutron imaging", in *Proc. 8th Int. Particle Accelerator Conf. (IPAC'17)*, Copenhagen, Denmark, May 2017, pp. 2533-2536. doi:10.18429/JACoW-IPAC2017-WE0BB3
- [5] G. H. Gillespie, <http://www.ghga.com/accelsoft/pbolab.html>
- [6] R. A. Marsh *et al.*, "High average power deuteron beam dynamics", in *Proc. 8th Int. Particle Accelerator Conf. (IPAC'17)*, Copenhagen, Denmark, May 2017, pp. 798-800. doi:10.18429/JACoW-IPAC2017-MOPIK112
- [7] R. A. Marsh, D. G. Gibson, and B. Rusnak, "Precision magnet measurements for deuteron beam transport", in *Proc. 9th Int. Particle Accelerator Conf. (IPAC'18)*, Vancouver, Canada, Apr.-May 2018, pp. 3670-3672. doi:10.18429/JACoW-IPAC2018-THPAL022
- [8] F. Becker, C. Andre, P. Forck, D. H. H. Hoffmann, and H. Iwase, "Profile measurement by beam induced fluorescence for 60 to 750 MeV/u heavy ion beams", in *Proc. 10th European Particle Accelerator Conf. (EPAC'06)*, Edinburgh, UK, Jun. 2006, paper TUPCH010, pp. 1013-1015.
- [9] A. Variola, R. Jung, and G. Ferioli, "Characterization of a nondestructive beam profile monitor using luminescent emission", *PRSTAB* 10, 122801 (2007).
- [10] J. M. Carmona, "Measurements of nonintercepting fluorescence profile monitor prototypes using 9 MeV deuterons", *PRAB* 15, 072801 (2012).
- [11] J. F. Ziegler, <http://www.srim.org/>